Spectral Response of Long-Period Fiber Grating Based on Tapered Fiber With Side-Contacted Metal Grating

Kuei-Chu Hsu, Nan-Kuang Chen, Cheng-Ling Lee, Yu-Syun Chih, Pei-Jhen Jhuang, Yinchieh Lai, and Chinlon Lin

***Abstract*—A new long-period fiber grating structure based on a tapered fiber side contacted with a metal grating is proposed and demonstrated in this paper. The temperature/index tuning sensitivity can be enhanced, and the unusual spectral response of decreasing phase-matching wavelength with respect to increasing grating period and temperature is observed.**

***Index Terms*—Fiber optics component, fiber optics sensors, gratings, optical fibers.**

I. Introduction

LONG-PERIOD FIBER GRATINGS (LPFGs) with artificial waveguiding structures or material constituents may possess larger wavelength tunability for sensing applications, and may have more functionalities than conventional LPFGs [1]–[10]. Conventional LPFGs are made by introducing periodic index changes in the fiber core to couple the core mode with cladding modes at discrete wavelengths [11]–[13]. In sensing applications, the conventional LPFGs have limited wavelength sensitivity of temperature and refractive index due to the tight mode-field confinement. Numerous kinds of LPFGs have been proposed to enhance the sensitivity, including the use of short-grating period [9], ultrathin cladding layer [10], asymmetric CO_2 laser ablation [3]–[5], and surface-corrugated fibers [6]. Among them, the fiber constituents with high thermo-optic coefficients and the strong overlap among the core mode, cladding modes, and the external medium are the most crucial factors to the tuning efficiency of the LPFG resonance wavelengths.

Manuscript received November 03, 2009; revised December 08, 2009. First published December 31, 2009; current version published March 05, 2010. This work was supported in part by the National Science Council of the Republic of China under Grant NSC 98-2218-E-008-004- and Grant NSC 96-2628-E-009-154-MY3.

K.-C. Hsu is with the Department of Optics and Photonics, National Central University, Jhong-Li 320, Taiwan (e-mail: kchsu@dop.ncu.edu.tw).

N.-K. Chen and C.-L. Lee are with the Department of Electro-Optical Engineering, and Optoelectronics Research Center, National United University, Miaoli 360, Taiwan.

Y.-S. Chih, P.-J. Jhuang, and Y. Lai are with the Department of Photonics and Institute of Electro-Optical Engineering, National Chiao Tung University, Hsinchu 300, Taiwan.

C. Lin is with the School of Electrical and Electronic Engineering, Nanyang Technological University, Singapore 639798, Singapore.

Color versions of one or more of the figures in this paper are available online at http://ieeexplore.ieee.org.

Digital Object Identifier 10.1109/JLT.2009.2039552

Since the conventional LPFGs have limited sensing ability due to the tight mode-field confinement, to enhance the sensitivity of the LPFGs, the tapered fiber is a good candidate to cause the field of the high-order modes more extend into the external medium. The strong interaction of the optical evanescent field with the environment can produce highly wavelength-dependent index sensing sensitivity between the fundamental mode and high-order modes, which, in turn, affects the phase-matching wavelengths and mode-coupling characteristics. The device is thus more sensitive to the index variation of the external medium. The slimmed down fiber with cylindrical symmetric surface-corrugated LPFGs had been proposed [6]. However, the dispersion-related sensing capability as well as the tuning response of the LPFGs based on slimmed down fibers have not been well investigated yet. In our previous work, high-efficiency, wideband-tunable, asymmetric laser-ablated long-period fiber gratings that use an optical polymer overlay was demonstrated [5]. However, in the viewpoint of using artificial waveguide structure to generate evanescent wave, which can enhance the sensitivity with the environmental change, tapered fibers can be further considered to be applied in our previous asymmetric LPFG structure. This is the motivation of this paper.

In this paper, we experimentally demonstrate a new LPFG structure based on a tapered fiber with a side-contacted metal grating to form a flexible and highly sensitive sensor. The proposed LPFG is composed of a fiber taper with a uniform waist and a side-contacted metal grating that provides an enhanced, but opposite dip wavelength tuning tendency with respect to the grating period and temperature change when compared to conventional LPFGs. The unusual temperature and refractive index tuning characteristics of the proposed LPFGs attribute to the unique material and waveguide dispersion characteristics of the proposed novel structure.

II. Experiment and Analysis

A. Mode Analysis of Tapered Fibers

Fig. 1(a) depicts the studied tapered fiber structure. The diameter D of the uniform waist is a few tens of micrometers and the length is approximately 1 cm, and the transition zone has an exponential shape ranging from 125 μm to D with the transition length around 1.75 cm. The evanescent waves spread out of the fiber and reach the external environment when the single-mode optical fiber is tapered down to a few tens of micrometers in diameter. The pure-silica cladding now plays as a new waveguide,

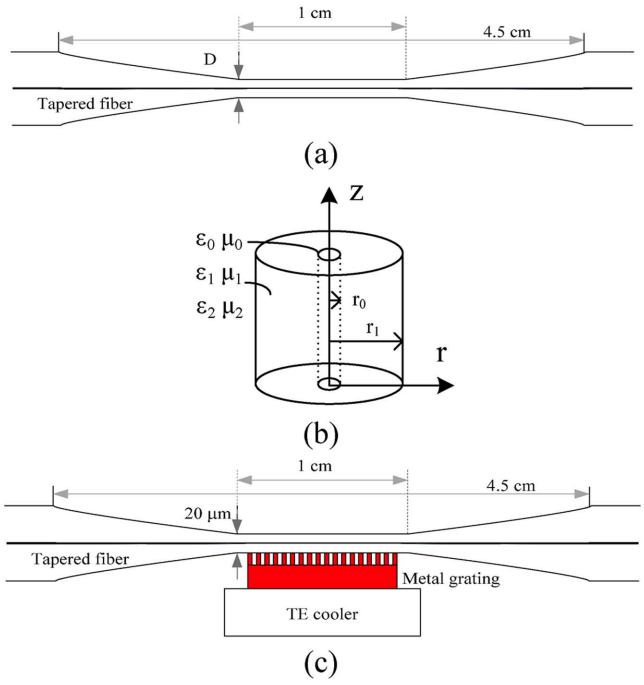

Fig. 1. (a) Diagram of the tapered optical fiber with a uniform waist. (b) Step profile of three-layer fiber. (c) Diagram of the LPEG composed of a tapered optical fiber with a uniform waist and a side-contacted metal grating.

and the optical fields are confined by the external medium as the cladding.

The analysis of mode propagation in tapered fibers takes account of the refractive index profile over the whole cross section and the taper geometry. Consider the fiber taper as a three-layer structure, which is composed of a core embedded in a finite cladding surrounded by an external medium. Since the cross section of a fiber taper is varying along the axis, there is no exact analytic solution of Maxwell's equations generally. There are several approaches to perform the analysis for such cases, but the concept of local modes is the most intuitive and simplest [14]. The concept of local modes assumes that the fiber taper is slowly varying, and the modes in a fiber taper at any point along the fiber axis are equal to the modes of a straight fiber with the same core diameter. Hence, the modes of such a straight fiber are approximations to the solutions of Maxwell's equations within local regions. In our devices, since the grating is side contacted with the waist of fiber taper, only the modes in the section of the uniform taper waist need to be calculated. Another assumption that we have made is that the ratio of the diameters of cladding and core remains constant during tapering, so that the tapered fiber structure can be determined. The step profile of the three-layer fiber is depicted in Fig. 1(b). The variables r_0 and r_1 are the radius of the core and cladding at the waist of the tapered fiber, respectively. The core with constitutive parameters μ_0 and ε_0 is embedded in the cladding with μ_1 and ε_1, which is surrounded by the external medium with μ_2 and ε_2. The field distributions and propagation constants of the modes can be obtained by solving the appropriate boundary-value problem of the wave-guiding equations. The wave-guiding equation for longitudinal components of the fields (E_z and H_z) in the cylindrical polar coordinates (r, φ, z) with the z axis along the axis of the fiber is given by

$$\left[\frac{1}{r}\frac{\partial}{\partial r}\left(r\frac{\partial}{\partial r}\right)+\frac{1}{r}\frac{\partial^2}{\partial\varphi^2}+k_r^2\right]\begin{Bmatrix}E_z\\H_z\end{Bmatrix}=0 \tag{1}$$

where $k_r^2=\omega^2\varepsilon\mu-k_z^2$. Inside the core, solutions for E_z and H_z are Bessel functions, which are given by

$$E_z=AJ_m(k_{r_0}r)\cos(m\phi)e^{ik_zz} \tag{2}$$
$$H_z=BJ_m(k_{r_0}r)\sin(m\phi)e^{ik_zz} \tag{3}$$

with $k_z^2+k_{r0}^2=\omega^2\varepsilon_0\mu_0$. In the cladding region, solutions for E_z and H_z are

$$E_z=CJ_m(k_{r_1}r)\cos(m\varphi)e^{ik_zz}+DY_m(k_{r_1}r)\cos(m\phi)e^{ik_zz} \tag{4}$$
$$H_z=FJ_m(k_{r_1}r)\sin(m\varphi)e^{ik_zz}+GY_m(k_{r_1}r)\sin(m\varphi)e^{ik_zz} \tag{5}$$

with $k_z^2+k_{r1}^2=\omega^2\varepsilon_1\mu_1$. In the surrounding, the field associated with the guiding wave is evanescent in the radial direction. By letting $k_{r1}=i\alpha_{r2}$, the solutions in the surrounding are

$$E_z=IH_m^{(1)}(i\alpha_{r_2}r)\cos(m\phi)e^{ik_zz} \tag{6}$$
$$H_z=JH_m^{(1)}(i\alpha_{r_2}r)\sin(m\phi)e^{ik_zz} \tag{7}$$

with $k_z^2+k_{r2}^2=\omega^2\varepsilon_2\mu_2$. In the aforementioned solutions, J_m and Y_m are the Bessel functions of the first and second kind, respectively, and $H_m^{(1)}$ is the Hankel function. There are eight coefficients, A, B, C, D, F, G, I, and J, to be solved by boundary conditions at interfaces between different dielectric media. The following four equations at $r=r_0$ are obtained:

$$AJ_m(k_{r_0}r_0)-CJ_m(k_{r_1}r_0)-DY_m(k_{r_1}r_0)=0 \tag{8}$$
$$BJ_m(k_{r_0}r_0)-FJ_m(k_{r_1}r_0)-GY_m(k_{r_1}r_0)=0 \tag{9}$$
$$A\frac{\omega\varepsilon_0}{k_{r_0}r_0}J_m'(k_{r_0}r_0)+B\frac{mk_z}{k_{r_0}^2r_0^2}J_m(k_{r_1}r_0)-C\frac{\omega\varepsilon_1}{k_{r_1}r_0}J_m'(k_{r_1}r_0)-D\frac{\omega\varepsilon_1}{k_{r_1}r_0}Y_m'(k_{r_1}r_0)-F\frac{mk_z}{k_{r_1}^2r_0^2}J_m(k_{r_1}r_0)-G\frac{mk_z}{k_{r_1}^2r_0^2}Y_m(k_{r_1}r_0)=0 \tag{10}$$
$$A\frac{mk_z}{k_0^2r_0^2}J_m(k_{r_0}r_0)+B\frac{\omega\mu_0}{k_{r_0}r_0}J_m'(k_{r_0}r_0)-C\frac{mk_z}{k_{r_1}^2r_0^2}J_m(k_{r_1}r_0)-D\frac{mk_z}{k_{r_1}^2r_0^2}Y_m(k_{r_1}r_0)-F\frac{\omega\mu_1}{k_{r_1}r_0}J_m'(k_{r_1}r_0)-G\frac{\omega\mu_1}{k_{r_1}r_0}Y_m'(k_{r_1}r_0)=0 \tag{11}$$

and the other four are obtained from boundary conditions at $r=r_1$ as

$$CJ_m(k_{r_1}r_1)+DY_m(k_{r_1}r_1)-IH_m(i\alpha_{r_2}r_1)=0 \tag{12}$$
$$FJ_m(k_{r_1}r_1)+GY_m(k_{r_1}r_1)-JH_m(i\alpha_{r_2}r_1)=0 \tag{13}$$

$$C\frac{\omega\varepsilon_1}{k_{r_1}r_1}J'_m(k_{r_1}r_1)+D\frac{\omega\varepsilon_1}{k_{r_1}r_1}Y'_m(k_{r_1}r_1)+F\frac{mk_z}{k_{r_1}^2r_1^2}J_m(k_{r_1}r_1)+G\frac{mk_z}{k_{r_1}^2r_1^2}Y_m(k_{r_1}r_1)+I\frac{i\omega\varepsilon_2}{\alpha_{r_2}r_1}H'_m(i\alpha_{r_2}r_1)+J\frac{mk_z}{\alpha_{r_2}^2r_1^2}H_m(i\alpha_{r_2}r_1)=0 \tag{14}$$

$$C\frac{mk_z}{k_{r_1}^2r_1^2}J_m(k_{r_1}r_1)+D\frac{mk_z}{k_{r_1}^2r_1^2}Y_m(k_{r_1}r_1)+F\frac{\omega\mu_1}{k_{r_1}^2r_1^2}J'_m(k_{r_1}r_1)+G\frac{\omega\mu_1}{k_{r_1}^2r_1^2}Y'_m(k_{r_1}r_1)+I\frac{mk_z}{\alpha_{r_2}^2r_1^2}H'_m(i\alpha_{r_2}r_1)+J\frac{i\omega\mu_2}{\alpha_{r_2}r_1}H'_m(i\alpha_{r_2}r_1)=0. \tag{15}$$

Equations (8)–(15) resulted from the continuity of E_z, H_z, and E_φ, H_φ give rise to the guidance conditions for the waveguide modes. Since the eight equations are a set of homogeneous linear equations, the determinant of the coefficient matrix has to be zero in order to have nonzero solutions. This condition is the final characteristic equation for determining the dispersion relation of the modes.

B. Phase-Matching Wavelength Analysis for LPFG With Side-Contacted Metal Grating Structure

An LPFG based on a tapered fiber with a side-contacted metal grating is shown in Fig. 1(c). A uniform taper waist around 20-μm diameter is achieved by tapering down a standard single-mode fiber (Corning SMF-28). The details of fabrication process have been addressed in our previous works [15]–[17]. The length of the uniform waist is around 1 cm, and the length of the taper transition region is approximately 1.75 cm. A 1-D thin-aluminum-layer grating of total length about 1 cm is side contacted with the taper fiber waist. The metal grating is put on a thermoelectric cooler (TE cooler) to control the temperature of the LPFG. The 20-μm-diameter waveguide can support many propagation modes as the *V* value is around 100. As the light source is launched in, the fundamental mode propagated along SMF-28 is adiabatically converted to the fundamental mode that propagates along the fiber taper. Mode coupling occurs in the metal grating contact region when the phase-matching condition is satisfied. The coupled high-order modes will escape totally after the second taper region, and thus, the attenuation dips in the transmission spectrum are produced.

The effective index of the fiber mode M_{ml} is denoted as $n_{\text{eff}-ml}$. Here, m denotes the angular order and l denotes the lth root of the modal characteristic equation solved from (8)–(15). In this way, $n_{\text{eff}-11}$ is the effective index of the fundamental mode. Fig. 2(a)–(c) displays the effective index difference $(n_{\text{eff}-11}-n_{\text{eff}-ml})$ as functions of the wavelength for D = 10, 20, and 30 μm, respectively. The fiber is assumed to be surrounded by air. The index difference between the air and the pure silica is so high that the mode field diameters of the cladding mode shrink to be well confined in the fiber for large *D*. For the same pair of coupled modes, the $(n_{\text{eff}-11}-n_{\text{eff}-ml})$ increases with decreasing taper diameter. This is because high fraction of the fields for the higher order modes leak more in the air for smaller *D*. To analyze the mode coupling effects in the studied LPFGs, the refractive index difference between the fundamental mode and seven high-order modes are solved and plotted in Fig. 2(a)–(d). The phase-matching condition can be expressed in terms of the intermodal dispersion function $\Phi(\lambda)$ defined by

$$\Phi(\lambda_{\text{m}})=\frac{2\pi(\text{n}_{\text{eff},1}-\text{n}_{\text{eff},2})}{\lambda_{\text{m}}}=\frac{2\pi}{\Lambda} \tag{16}$$

where $\text{n}_{\text{eff},1}$ and $\text{n}_{\text{eff},2}$ are effective indexes of the two coupled modes, λ_m is the phase-matching wavelength to be determined, and Λ is the grating period. The phase-matching wavelengths can be determined graphically as the intersections of the intermodal dispersion function with the grating spatial frequency $2\pi/\Lambda$. However, since the proposed asymmetric LPFG structure, as shown in Fig. 4, should somehow affect the symmetric mode shapes of the taper fibers, the actual intermodal dispersion may be slightly different for practical devices.

As aforementioned, the crossed points of the $(n_{\text{eff}-11}-n_{\text{eff}-ml})/\lambda$ curve and the constant $1/\Lambda$ curve denote the phase-matching wavelengths at a specific grating period. Fig. 2(d) shows the $(n_{\text{eff}-0}-n_{\text{eff}-m})$ for $D=20$ μm and the fiber is now assumed to be surrounded by the optical liquids (Cargille index-matching liquids with the index $n_D=1.43$). The mode fields now highly spread out of the optical fiber waist when propagate in the taper surrounded by the optical liquids due to the small index difference. This causes smaller $(n_{\text{eff}-11}-n_{\text{eff}-ml})$ compared to that shown in Fig. 2(b). For the grating period around 200–500 μm, the $(n_{\text{eff}-11}-n_{\text{eff}-ml})/\lambda$ is from 2.0×10^{-3} to 5.0×10^{-3} at $\lambda=1.55$ μm. As can be seen in Fig. 2(b), the waist diameter of $D=20$ μm is suitable for lower order mode coupling at the given metal grating period (200–500 μm) in this paper. For illustration purposes, to compare the influence of taper waist diameter on intermodal coupling, Fig. 3(a) plots the intermodal dispersion of coupled modes between M_{11} and M_{14} for different taper diameters. The value of $(n_{\text{eff}-11}-n_{\text{eff}-14})/\lambda$ increases with decreasing waist diameter, and the slope of intermodal dispersion of coupled modes becomes steeper for smaller waist diameters. Figs. 2 and 3 show that the resonance wavelength should be highly sensitive to the grating period change at a larger waist diameter for lower order mode coupling.

Again, for illustration purposes, Fig. 3(b) plots the M_{11}–M_{01} intermodal dispersion for the untapered SMF-28 fiber surrounded by the air as well as for the tapered fibers with different surrounding media. It has been known that there are two types of LPFGs: one is the positive linear-dispersion grating $(d\lambda_m/d\Lambda>0)$, and the other is the negative linear-dispersion grating $(d\lambda_m/d\Lambda<0)$. The conventional LPFGs with periodic index changes along the fiber core of the standard single-mode fiber are positive linear-dispersion gratings, while the proposed LPFGs shown in Fig. 2(a)–(d) are negative linear-dispersion gratings. The SMF-28 has steeper slope of $(n_{\text{eff}-11}-n_{\text{eff}-ml})/\lambda$ than the tapered fiber does, as shown in Fig. 3(b), indicating that the phase-matching wavelengths of conventional LPFGs is less sensitive than that of proposed

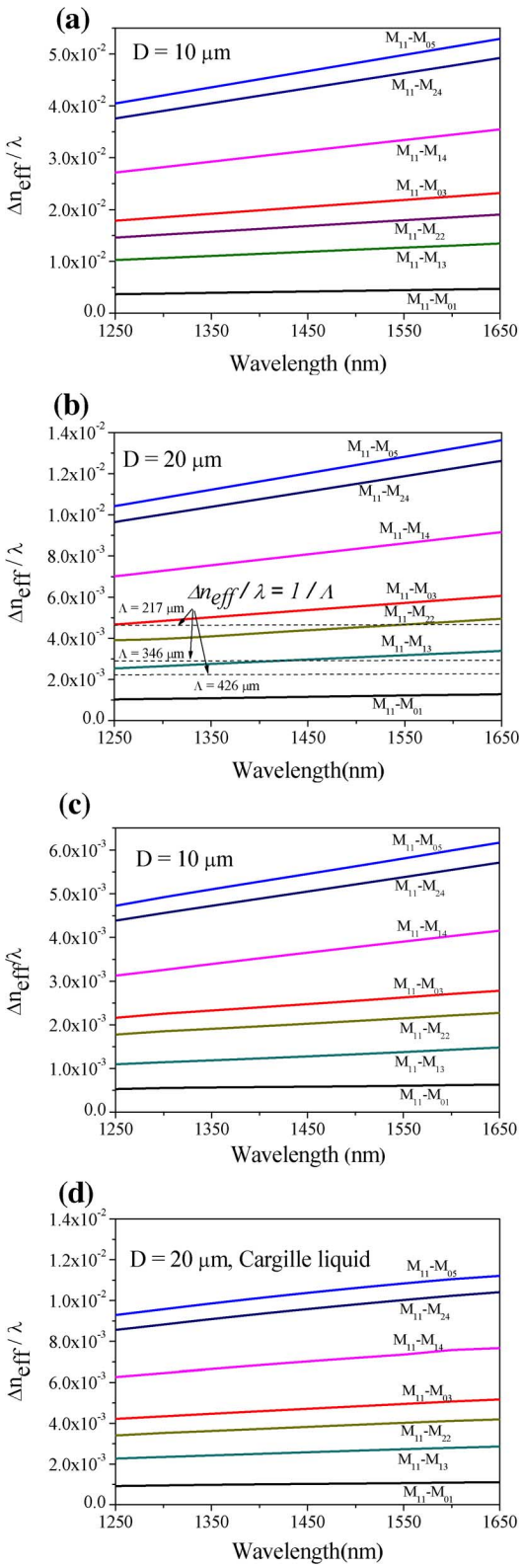

Fig. 2. (a)–(c) Simulation results of index difference for taper waist diameters equal to 10, 20, and 30 μm and surrounded by air. (d) Simulation results of index difference for taper waist $\mathrm{diameter} = 20\,\mu$m and surrounded by Cargille liquid. D is waist diameter and Λ is grating period.

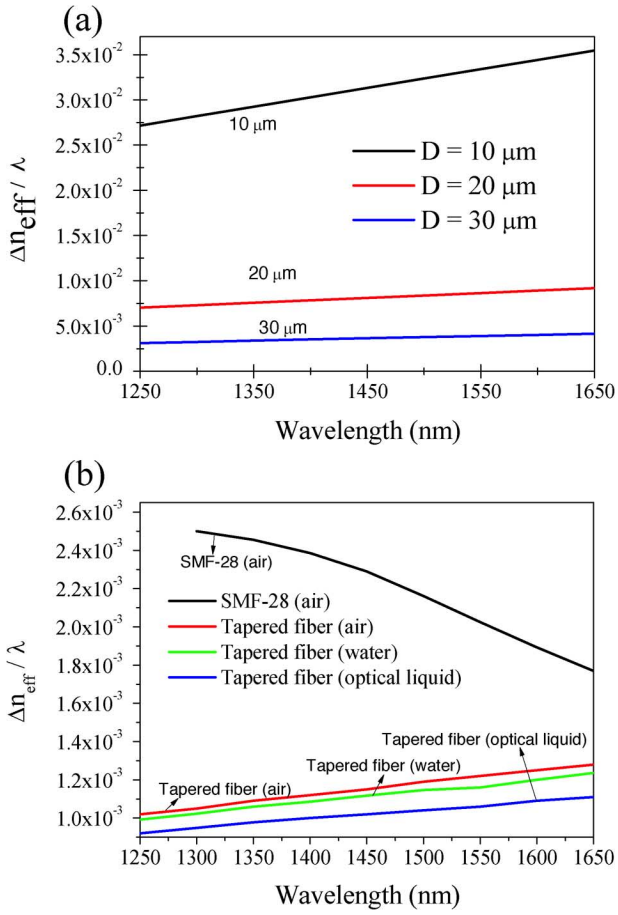

Fig. 3. (a) Simulation results of intermodal dispersion of coupled modes M_{11} and M_{14} of different taper diameter. (b) Intermodal dispersion of coupled modes M_{11} and M_{01} of the SMF-28 surrounded by air and the fiber taper with different surrounding media with $\mathrm{D} = 20\,\mu$m.

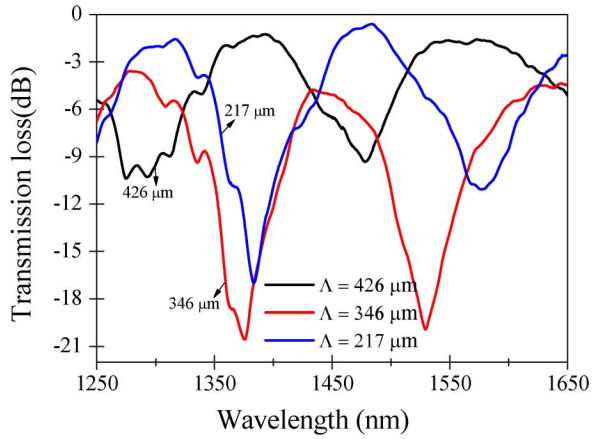

Fig. 4. Experimental result of transmission spectra of the LPFGs in the air with different periods with $D = 20\,\mu$m.

LPFGs. For the proposed LPFGs, fiber tapers with different surrounding media have different values of $(n_{\mathrm{eff}-11} - n_{\mathrm{eff}-ml})/\lambda$ and slightly different slope of intermodal dispersion. At the same waist diameter and grating period, increasing the refractive index of surrounding media will increase the resonance wavelength, as can be seen in Fig. 3(b). The negative slope of the $(n_{\mathrm{eff}-11} - n_{\mathrm{eff}-ml})$ with respect to wavelength due to the tapered-fiber-induced dispersion engineering will lead to interesting phenomena of the unusual wavelength tuning

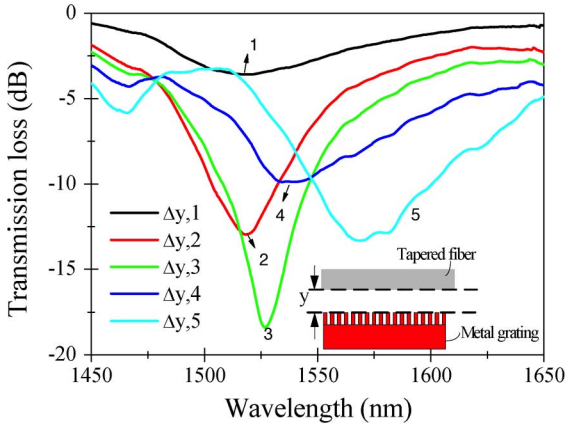

Fig. 5. Experimental result of transmission spectra of the LPFGs in the air at different separations from metal grating to tapered fiber with $D = 20\,\mu$m and grating $\mathrm{period} = 346\,\mu$m.

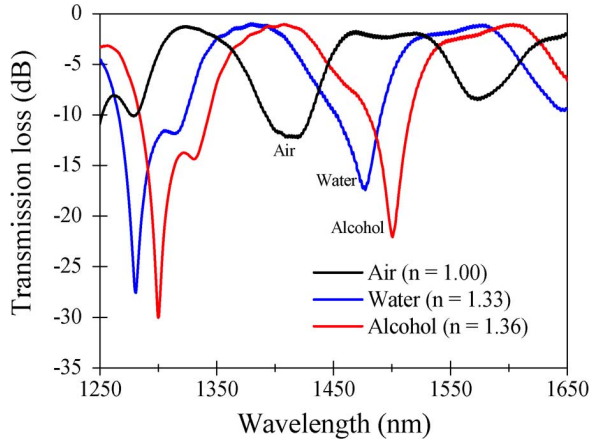

Fig. 6. Experimental transmission spectra of the LPFG device at room temperature in the air, water, and alcohol with the metal grating pitch of 426 μm.

tendency with respect to the grating period and temperature. These will be verified experimentally in the following section.

C. Measurement Results and Sensing Capability

Fig. 4 plots the experimental spectral responses of the proposed LPFGs under different grating periods at $D = 20\ \mu$m in the air at room temperature. As the grating period increases, the phase-matching wavelength decreases. Therefore, the proposed LPFG structure possesses opposite dip wavelength tuning tendency with respect to the period change when compared to conventional LPFGs. This experimental observation agrees with the theoretical analysis revealed in the previous section. However, the predicted phase-matching wavelengths (the cross point of $\Delta n_{\mathrm{eff}}/\lambda$ with $1/\Lambda$) shown in Fig. 2(b) may be different from the actual transmission dip wavelengths of the experimental data shown in Fig. 4. This is because the proposed side-contacted grating structure is different from the simulated symmetric tapered fiber structure, and thus, the mode profiles and effective indexes of modes may be slightly different from the solutions of (8)–(15). However, the predicted tuning tendency should not be affected by these uncertainties, as have been verified by the experimental data.

Fig. 5 shows the experimental transmission spectra of the LPFGs surrounded by the air with different separations from the metal grating to the tapered fiber waist with $D = 20\ \mu$m and grating $\mathrm{period} = 346\,\mu$m at room temperature. The marked lines labeled from $\Delta y, 1$ to $\Delta y, 5$, respectively, indicate the five cases of different distance change from the metal grating to the taper waist. The distance change is around 0.2 mm at each step, as shown in Fig. 5 (inset). When the waist of the tapered fiber moves closely to the metal grating, the phase-matching wavelength will shift to long wavelengths and the dip depth changes as well. The wavelength shift and dip depth change may be due to the change of the effective indexes difference between the two coupling modes, indicating that the effective indexes of the associated modes are modified because larger portion of the evanescent waves now interact with the metal grating when the tapered fiber moves more closely to the metal grating.

The experimental transmission spectra of the LPFG device at room temperature in the air with the metal grating pitch of 426 μm is shown in Fig. 6. When the water and alcohol are applied to cover the uniform waist section of the LPFGs, the two adjacent transmission dips gradually grow up and shift to longer wavelengths, as also shown in Fig. 6. Note that with the refractive index of the environmental material increases from water ($n = 1.33$) to alcohol ($n = 1.36$), the transmission dips apparently shift to longer wavelengths. These experimental results again are in good agreement with the theoretical analysis revealed in the previous section. Compare to the LPFG devices with the same surrounding medium reported in [4], our proposed LPFGs not only have more superior index sensing characteristics, but also have opposite wavelength shift tendency with respect to the increasing refractive index of the surrounding medium. The modes will spread more out of the taper region when the LPFGs are surrounded by the optical liquids instead of the air. Therefore, the overlap among the fundamental mode, higher order modes, and the grating is improved when the LPFGs are surrounded by the optical liquids. In this way, the transmission dip depth is increased due to stronger coupling. The environmental sensitivity of the phase-matching wavelengths is also enhanced in these cases.

To investigate the spectral responses of the LPFG at different heating temperatures, a metal grating with period of 217 μm is employed with the tapered fiber diameter $D = 20\ \mu$m. The applied temperature T ranges from 25 °C to 75 °C, and the spectral responses are shown in Fig. 7. The phase-matching wavelength moves to the short wavelength side and the peak attenuation gradually increased with increasing T. The grating pitch increases with increasing T for conventional LPFGs, and the phase-matching wavelength is changed to longer wavelengths at higher environmental temperature. In this conventional LPFG case, the tuning efficiency substantially depends on the thermal expansion coefficient of the fiber material. However, our proposed LPFGs have decreasing resonance wavelength with respect to the increasing temperature, and the average temperature tuning efficiency η is estimated to be about -0.24 nm/°C, which is greatly improved when compared to that of conventional LPFGs ($+0.06$ nm/°C [13]). The opposite temperature tuning tendency of the attenuation dip wavelength of the proposed LPFGs is due to the dispersion-engineered waveguiding

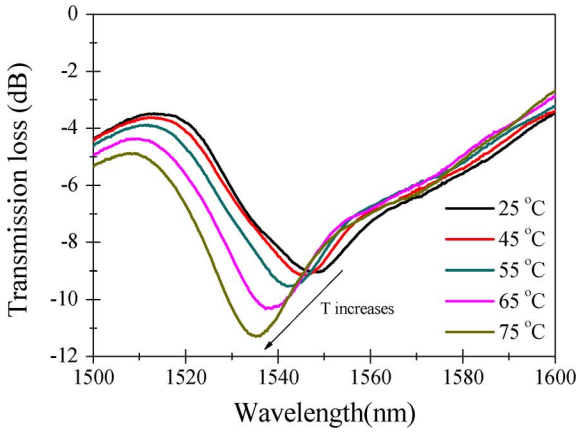

Fig. 7. Experimental transmission spectra of the LPFGs in the air at different temperatures with $D = 20\ \mu$m and grating $\text{period} = 217\ \mu$m.

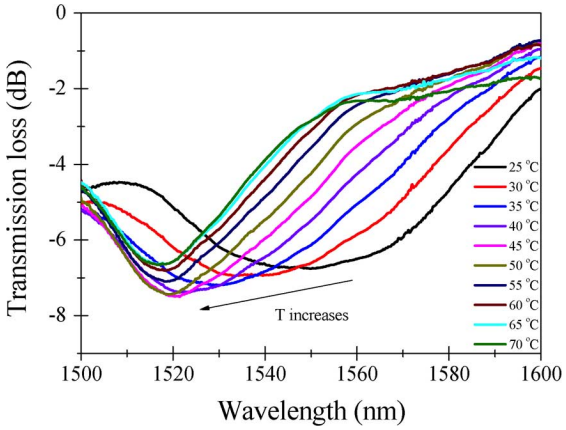

Fig. 8. Experimental transmission spectra of the LPFGs with $D = 20\ \mu$m, grating $\text{period} = 217\ \mu$m, and the surrounding medium is the heated Cargille index-matching liquids with the index $n_D = 1.43$ at room temperature.

structure that produces highly temperature-dependent dispersion characteristics between the coupling modes.

Besides observing the temperature tuning efficiency of the proposed LPFGs in the air, an optical liquid (Cargille index-matching liquids with the index $n_D = 1.43$ and the thermo-optic coefficient $dn_D/dT = -3.74 \times 10^{-4}/°\text{C}$) has also been applied to cover the uniform tapered section and the metal grating to observe the temperature tuning efficiency with the given surrounding media. Fig. 8 shows the wavelength shift of the LPFG surrounded by the optical liquids with varying *T*. From 25 °C to 70 °C, the phase-matching wavelength moves toward shorter wavelengths with increasing *T*. The optical liquid has a larger thermo-optic coefficient than the air and aluminum. The decreasing external refractive index makes $n_{\text{eff}-ml}$ decrease and $(n_{\text{eff}-11} - n_{\text{eff}-ml})$ increase at the same time. Thus, when compared with Fig. 6, a even larger wavelength shift shown in Fig. 8 is produced as a result of the higher thermo-optic coefficient of the optical liquids.

According to Figs. 5–7, the proposed LPFG is apparently sensitive to the applied tension, environmental index, and temperature variation. Therefore, for sensing applications, environmental fluctuations including tension, temperature, and index change, all can cause the resonance wavelength shift. It will be

TABLE I
COMPARISON OF INTERMODAL DISPERSION OF COUPLED MODES M_{11} AND M_{01} OF THE SMF-28 SURROUNDED BY AIR AND THE FIBER TAPER WITH SIDE-CONTACTED METAL GRATING UNDER DIFFERENT SURROUNDING MEDIA. $\Delta(l/\Lambda) = A_0 \Delta\lambda_m$

SMF-28 (Air)	Fiber taper (AIR)	Fiber taper (Water)	Fiber taper (Optical liquids, n_D = 1.42)
A_0 = -0.0032	A_0 = 0.0006	A_0 = 0.000548	A_0 = 0.000463

TABLE II
COMPARISON OF SENSITIVITY WITH GRATING PERIOD FOR VARIOUS KINDS OF LPFGS

	Conventional LPFGs	CO_2 laser exposed asymmetric LPFGs	Proposed LPFGs
Sensitivity (nm / R.I.U)	~ 40	~ 201	~ 640

difficult to selectively distinguish the individual effect without additional measurement. To prevent the selectivity problem, the proposed fiber optic sensor should either be designed to work under the change of only one environmental variable or some compensation schemes have to be used for taking into account the changes of other environmental variables.

To summarize the sensing characteristics, the comparison between conventional LPFGs and the proposed LPFG are presented in Tables I and II. Table I lists the comparison of the intermodal dispersion coefficients for the coupled modes M_{11} and M_{01} of the untapered SMF-28 fiber surrounded by air and the fiber taper with side-contacted metal grating under different surrounding media. Equation (17) describes the change of the phase-matching wavelength with respect to the grating period of LPFGs, where A_0 is the proportional coefficient listed in Table I. A smaller A_0 indicates larger sensitivity with respect to the period change

$$\Delta\frac{1}{\Lambda} = A_0 \Delta\lambda_m. \tag{17}$$

The conventional LPFGs are positive linear-dispersion gratings, while the proposed LPFGs immersed in different media are negative linear-dispersion gratings. The higher index of surrounding material makes the coefficient A_0 smaller, meaning the more sensitive wavelength tuning capability with respect to the grating period. Table II lists the refractive index sensitivity comparison [in units of nanometers/refractive index unit (R.I.U.)] of various kinds of LPFGs. Again, the sensitivity of the proposed LPFGs can be much greater than that of the conventional LPFGs.

III. CONCLUSION

In conclusion, a new LPFG structure based on a tapered fiber structure with a side-contacted metal grating to form a flexible and high-sensitivity sensing device has been demonstrated. In combination with the fiber tapering techniques, the evanescent fields of the fiber modes can directly interact

with the environment, which, in turn, directly affects the mode-coupling characteristics. In particular, the unusual spectral response of decreasing phase-matching wavelength with respect to the increasing grating period and temperature has been experimentally observed and theoretically analyzed. The temperature/index tuning sensitivity can be enhanced by suitably engineering the waveguide dispersion through tapering and employing suitable external materials.

REFERENCES

[1] S. Oh, K. R. Lee, U.-C. Paek, and Y. Chung, "Fabrication of helical long-period fiber gratings by use of a CO2 laser," *Opt. Lett.*, vol. 29, no. 13, pp. 1464–1466, 2004.

[2] Y. Liu, K. S. Chiang, Y. J. Rao, Z. L. Ran, and T. Zhu, "Light coupling between two parallel CO2-laser written long-period fiber gratings," *Opt. Exp.*, vol. 15, no. 26, pp. 17645–17651, 2007.

[3] M. Yan, S. Luo, L. Zhan, Z. Zhang, and Y. Xia, "Triple-wavelength switchable Erbium-doped fiber laser with cascaded asymmetric exposure long-period fiber gratings," *Opt. Exp.*, vol. 15, no. 7, pp. 3685–3691, 2007.

[4] T. Zhu, Y. J. Rao, J. L. Wang, and Y. Song, "A highly sensitive fiber-optic refractive index sensor based on an edge-written long-period fiber grating," *IEEE Photon. Technol. Lett.*, vol. 19, no. 24, pp. 1946–1948, Dec. 2007.

[5] N. K. Chen, D.-Y. Hsu, and S. Chi, "Widely tunable asymmetric long-period fiber grating with high sensitivity using optical polymer on laser-ablated cladding," *Opt. Lett.*, vol. 32, no. 15, pp. 2082–2084, 2007.

[6] W. Ding and S. R. Andrews, "Modal coupling in surface-corrugated long-period-grating fiber tapers," *Opt. Lett.*, vol. 33, no. 7, pp. 717–719, 2008.

[7] H. W. Lee and K. S. Chiang, "CO2 laser writing of long-period fiber grating in photonic crystal fiber under tension," *Opt. Exp.*, vol. 17, no. 66, pp. 4533–4539, 2009.

[8] Y. Liu and K. S. Chiang, "CO2 laser writing of long-period fiber gratings in optical fibers under tension," *Opt. Lett.*, vol. 33, no. 17, pp. 1933–1935, 2008.

[9] H. J. Patrick, A. D. Kersey, and F. Bucholtz, "Analysis of the response of long period fiber gratings to external index of refraction," *J. Lightw. Technol.*, vol. 16, no. 9, pp. 1606–1612, 1998.

[10] K. W. Chung and S. Yin, "Analysis of a widely tunable long-period grating by use of an ultrathin cladding layer and higher-order cladding mode coupling," *Opt. Lett.*, vol. 29, no. 8, pp. 812–814, 2004.

[11] A. M. Vengsarkar, P. J. Lemaire, J. B. Judkins, V. Bhatia, T. Erdogan, and J. E. Sipe, "Long-period fiber gratings as band rejection filters," *J. Lightw. Technol.*, vol. 14, no. 3, pp. 58–65, 1996.

[12] S. W. James and R. P. Tatam, "Optical fibre long-period grating sensors: Characteristics and application," *Meas. Sci. Technol.*, vol. 14, pp. R49–R61, 2003.

[13] J. A. Besley, T. Wang, and L. Reekie, "Fiber cladding mode sensitivity characterization for long-period gratings," *J. Lightw. Technol.*, vol. 21, no. 3, pp. 848–853, 2003.

[14] A. W. Synder and J. D. Love, *Oprical Waveguide Theory*. London, U.K.: Chapman & Hall, 1983.

[15] N. K. Chen, K. C. Hsu, S. Chi, and Y. Lai, "Tunable Er3+-doped fiber amplifiers covering S and C + L bands over 1490–1610 nm based on discrete fundamental-mode cutoff filters," *Opt. Lett.*, vol. 31, no. 19, pp. 2842–2844, Oct. 2006.

[16] S. Y. Chou, K. C. Hsu, N. K. Chen, S. K. Liaw, Y. S. Chih, Y. Lai, and S. Chi, "Analysis of thermo-optic tunable dispersion-engineered short-wavelength-pass tapered-fiber filters," *J. Lightw. Technol.*, vol. 27, no. 13, pp. 2208–2215, Jul. 2009.

[17] K. C. Hsu, N. K. Chen, S. Y. Chou, S. K. Liaw, Y. Lai, and S. Chi, "Bandpass filter with variable bandwidth based on a tapered fiber with external polymer cladding," *IEEE Photon. Technol. Lett.*, vol. 21, no. 13, pp. 935–937, Jul. 2009.

Kuei-Chu Hsu received the Ph.D. degree in electro-optical engineering from the National Chiao-Tung University, Hsinchu, Taiwan, in 2007.

In 2009, she joined the Faculty of the Department of Optics and Photonics, National Central University, Jhongli, Taiwan, where she is currently an Assistant Professor. Her research interests include fiber sensors and fiber lasers, liquid crystal optics, photonic crystals, and optical communications.

Nan-Kuang Chen, photograph and biography not available at the time of publication.

Cheng-Ling Lee received the Ph.D. degree from the Institute of Electro-Optical Engineering, National Chiao Tung University, Hsinchu, Taiwan, in 2003.

She is currently an Associate Professor in the Department of Electro-Optical Engineering, National United University, Miaoli, Taiwan, where she is also with the Optoelectronics research Center. Her research interests include fiber-grating synthesis, fiber-based devices, optical thin-film coatings, and optimization algorithms.

Yu-Syun Chih, photograph and biography not available at the time of publication.

Pei-Jhen Jhuang, photograph and biography not available at the time of publication.

Yinchieh Lai received the B.S. degree in electrical engineering from the National Taiwan University, Taipei, Taiwan, in 1985, and the M.S. and Ph.D. degrees in electrical engineering from Massachusetts Institute of Technology, Cambridge, in 1989 and 1991, respectively.

In 1991, he joined the Faculty of the Department of Photonics and Institute of Electro-Optical Engineering, National Chiao-Tung University, Hsinchu, Taiwan, where he is currently a Professor. His research interests include quantum nonlinear optical pulse propagation, nonlinear optics, modelocked fiber lasers, and fiber devices.

Chinlon Lin, photograph and biography not available at the time of publication.